Cellular/Molecular

Dynamin 1 Restrains Vesicular Release to a Subquantal Mode In Mammalian Adrenal Chromaffin Cells

Qihui Wu,* Quanfeng Zhang,* Bin Liu, Yinglin Li, Xi Wu, Shuting Kuo, Lianghong Zheng, Changhe Wang, Feipeng Zhu, and Zhuan Zhou

State Key Laboratory of Membrane Biology and Beijing Key Laboratory of Cardiometabolic Molecular Medicine, Institute of Molecular Medicine and Peking-Tsinghua Center for Life Sciences and Peking University–IDG/McGovern Institute for Brain Research, Peking University, Beijing 100871, China

Dynamin 1 (dyn1) is required for clathrin-mediated endocytosis in most secretory (neuronal and neuroendocrine) cells. There are two modes of Ca^{2+}-dependent catecholamine release from single dense-core vesicles: full-quantal (quantal) and subquantal in adrenal chromaffin cells, but their relative occurrences and impacts on total secretion remain unclear. To address this fundamental question in neurotransmission area using both sexes of animals, here we report the following: (1) dyn1-KO increased quantal size (QS, but not vesicle size/content) by ≥250% in dyn1-KO mice; (2) the KO-increased QS was rescued by dyn1 (but not its deficient mutant or dyn2); (3) the ratio of quantal versus subquantal events was increased by KO; (4) following a release event, more protein contents were retained in WT versus KO vesicles; and (5) the fusion pore size (d_p) was increased from ≤9 to ≥9 nm by KO. Therefore, Ca^{2+}-induced exocytosis is generally a subquantal release in sympathetic adrenal chromaffin cells, implying that neurotransmitter release is generally regulated by dynamin in neuronal cells.

Key words: **dynamin; fusion pore; kiss-and-run; neurotransmitter release; quantal; subquantal**

Significance Statement

Ca^{2+}-dependent neurotransmitter release from a single vesicle is the primary event in all neurotransmission, including synaptic/neuroendocrine forms. To determine whether Ca^{2+}-dependent vesicular neurotransmitter release is "all-or-none" (quantal), we provide compelling evidence that most Ca^{2+}-induced secretory events occur via the subquantal mode in native adrenal chromaffin cells. This subquantal release mode is promoted by dynamin 1, which is universally required for most secretory cells, including neurons and neuroendocrine cells. The present work with dyn1-KO mice further confirms that Ca^{2+}-dependent transmitter release is mainly via subquantal mode, suggesting that subquantal release could be also important in other types of cells.

Introduction

Sixty-four years ago, Bernard Katz proposed that presynaptic transmission is mediated as "all-or-none" neurotransmitter release (Del Castillo and Katz, 1954). Until recently, this quantal hypothesis has been one of the central concepts in synaptic transmission between neurons (Matsuda et al., 2009; Zhang et al., 2009), as well as neurotransmitter release from adrenal chromaffin cells (ACCs), a cell model for neuronal secretion studies (Chow et al., 1992; Chen et al., 2005; Zhao et al., 2016). Similar to neurotransmitter release in neurons (Neher and Sakaba, 2008), ACCs release catecholamine from large dense-core vesicles (LDCVs) following an increase in intracellular Ca^{2+} (Crivellato et al., 2008). Transmitter release from individual LDCVs or synaptic vesicles can be recorded as quantal spike (or foot + spike) by electrochemical amperometry using a micro carbon fiber electrode (CFE) (Wightman et al., 1991; Chow et al., 1992; Alvarez de Toledo et al., 1993; Zhou and Misler, 1995a; Huang et al., 2007). In nonexcitable mast cells, there are two types of vesicle fusion modes, "full-fusion-like" (FFL) and "fusion pore flickering"/"kiss-and-run" (KAR) modes (Alvarez de Toledo et al., 1993). In principle, a KAR fusion event can produce both subquantal and full-quantal modes depending on whether the fusion pore closes before all native (or false) transmitters are discharged.

Received May 11, 2018; revised Oct. 14, 2018; accepted Oct. 15, 2018.

Author contributions: Z.Z. designed the research; Q.W., Q.Z. and B.L. performed research and analyzed data; Y.L., X.W., S.K., L.Z. performed research; Z.Z., Q.W., Q.Z., C.W. and F.Z. wrote paper.

This work was supported by the National Key Research and Development Program of China (Grant 2016YFA0500401), the National Natural Science Foundation of China (Grants 31330024, 31761133016, 21790394, 31171026, 31327901, 31521062, and 21790390), and the National Basic Research Program of China (Grant 2012CB518006). We thank Jianhua Xu (Georgia Regents University), Jianyuan Sun (Chinese Academy of Sciences Institute of Biophysics), and Iain C. Bruce (Peking University) for reading this manuscript.

The authors declare no competing financial interests.

*Q.W. and Q.Z. contributed equally to this work.

Correspondence should be addressed to Dr. Zhuan Zhou, Institute of Molecular Medicine, Peking University, 5 Yiheyuan Road, Beijing 100871, China. E-mail: zzhou@pku.edu.cn.

https://doi.org/10.1523/JNEUROSCI.1255-18.2018

 0270-6474/19/390199-13$15.00/0

Using modified low-noise CFEs to record Ca^{2+}-dependent single vesicle release in excitable chromaffin cells, we reported two types of native neurotransmitter release modes, the "stand-alone foot" (subquanta) and "foot + spike" (full-quanta) (Zhou et al., 1996), which have been confirmed by others (Albillos et al., 1997; Alés et al., 1999; Elhamdani et al., 2001). Subsequently, GPCR-Gi-$\beta\gamma$ is found as a signaling pathway regulates the vesicle release modes between subquanta and full quanta (Chen et al., 2005; Gerachshenko et al., 2009). In addition, dynamin 1 (dyn1), a GTPase required for clathrin-mediated endocytosis and membrane remodeling in neurons and endocrine cells (Ferguson et al., 2007), has been implicated, using pharmacology, antibodies, and phosphorylation, in the release modes in ACCs (Elhamdani et al., 2001; Chen et al., 2005; González-Jamett et al., 2010; Ferguson and De Camilli, 2012; Samasilp et al., 2012; Jackson et al., 2015; Ren et al., 2016). Intracellular dialysis of a peptide derived from the proline-rich domain of dynamin eliminates the regulation of quantal size by Gi-$\beta\gamma$, suggesting that dyn1 directly regulates quantal size (Chen et al., 2005). These experiments, however, suffer from possible off-target effects of the pharmacological manipulation of dyn1. To date, most studies on the mechanisms of subquantal release (or KAR vesicle fusion) have used cell lines (Pothos et al., 1998; Larsen et al., 2006; Westerink and Ewing, 2008; Mellander et al., 2012; Ren et al., 2016), so their results require critical confirmation in native secretory cells. In a few studies, effects of dyn1 overexpression or RNAi have used native ACCs, but unfortunately they lack controls (rescue or scrambled RNAi) for possible transfection artifacts (Anantharam et al., 2011; González-Jamett et al., 2013). Therefore, to determine the extent to which dyn1 is involved in exocytosis, it is essential to use the gold standard of loss of function and rescue of dyn1 in native dyn1-KO ACCs.

To determine the role of the subquantal mode in evoked catecholamine release, we determined whether dyn1 regulates subquantal release in native mouse ACCs using several single-vesicle assays [CFEs, total internal reflection fluorescence (TIRF) microscopy, electron microscopy (EM), and single-vesicle imaging of dextran uptake]. We found that, in contrast to the WT, dyn1-KO increased the largest quantal size by 250% and this was rescued by overexpressing dyn1-WT, but not a functionally deficient dyn1 mutant or WT dynamin 2 (dyn2). Therefore, dyn1 maintains most releasing vesicles in the subquantal mode (<40% of total content) by rapid resealing of the fusion pore before complete release of catecholamine in native ACCs.

Materials and Methods

Cell culture, transfection, and plasmids. The use and care of animals were approved and directed by the Institutional Animal Care and Use Committee of Peking University and the Association for Assessment and Accreditation of Laboratory Animal Care. dyn1-KO mice were kindly provided by Dr. Pietro De Camilli. We used dyn1-KO mice on postnatal days 2 (P2) to P5 because dyn1-KO mice can survive only ≤5 d after birth (Ferguson et al., 2007; Kuo et al., 2014). The mice were killed by hypothermic anesthesia on ice for 2 min. Both males and females were used in our experiments. Mouse ACCs were cultured as described previously with minor modifications (Albillos et al., 1997). Briefly, the adrenal glands were isolated from an anesthetized animal and then incubated in papain solution for 40 min at 37°C after removing the cortex. Cells were then dissociated by trituration and transfected with 3 μg of NPY-pHluorin-expressing plasmids using the Neon (10 μl) electroporation system (MPK1096, Invitrogen) according to the manufacturer's instructions. The transfected cells were plated on poly-L-lysine-coated coverslips and cultured for 18–48 h in a humidified incubator (37°C, 5% CO_2) before use. The WT and KO cells from littermate mice were cultured and experimented under same conditions. NPY-pHluorin plasmid was constructed as described previously (Wang et al., 2017). NPY-mCherry was constructed by substituting pHluorin with mCherry. The dynamin 2 plasmid was a kind gift from Dr. Ana M. Cárdenas (Universidad de Valparaíso, Chile). All chemicals were from Sigma-Aldrich unless otherwise indicated.

Adrenal slice preparation. Adrenal slices were prepared according to previous reports (Chen et al., 2008) with minor modifications. Briefly, adrenal glands were removed from neonatal mice and immediately placed in ice-cold "slice solution" containing the following (in mM): 125 NaCl, 2.5 KCl, 2 $CaCl_2$, 1 $MgCl_2$, 1.25 NaH_2PO_4, 26 $NaHCO_3$, and 10 glucose, pH 7.4, after gassing with 95% O_2 mixed with 5% CO_2. The slice solution was used as the extracellular medium in the CFE recordings. When 70 mM K was used as a secretagogue, it replaced an equimolar amount of NaCl in the cutting solution. After removing overlying fatty tissue, the glands were embedded in 3% agarose (type VII-A, low-melting-point agarose) and cut into slices (150 μm thick) using a vibrating-blade microtome (Leica 1200). The slices were kept for 10 min at 37°C in a holding chamber containing cutting solution and then at room temperature. Slices were used for up to 12 h after cutting.

Electrochemical recordings. We used a standard patch-clamp amplifier (Yibo) for CFE (7 μm diameter, ProCFEs, Dagan) recordings as described previously (Zhou and Misler, 1995b). CFE recordings were sampled at 5 kHz, low-pass filtered at 1 kHz, and digitized at 2–5 kHz. The top 75% of the largest events in each cell were analyzed for statistics. Igor software (Wavemetrics) and a custom-made macro-software (Zhou et al., 1996) were used for all offline data analysis. All experiments were performed at room temperature unless otherwise indicated.

TIRF imaging and analysis. TIRF imaging was performed on an inverted microscope with a 100× TIRF objective lens (Olympus IX-81; numerical aperture 1.45). Images were captured by an Andor EMCCD using Andor iQ software with an exposure time of 50 ms. The standard bath solution contained the following (in mM): 145 NaCl, 2.8 KCl, 2 $CaCl_2$, 1 $MgCl_2.6H_2O$, 10 H-HEPES, and 10 D-glucose, pH 7.4. The temperature was kept at ~35°C by a laboratory-made heater throughout all TIRF experiments. To distinguish between fusion events and vesicle movement, exocytotic events were defined as abrupt fluorescence increases immediately followed by a decrease or diffusion of NPY-pHlourin or BDNF-pHluorin puncta in the vicinity. In the analysis of single release events, each event was selected and marked with 1.92 μm (center) and 2.4 μm (annulus) diameter circular areas, following earlier reports (Bowser and Khakh, 2007; Wang et al., 2017). This "center and annulus" method for separating KAR and FFL events has been established in astrocytes (Bowser and Khakh, 2007) and DRG neurons (Wang et al., 2017) and it also works in chromaffin cells (see Fig. 4; also see examples from Movies 1, 2, 3 and 4, where FFL events with annulus "puffs" are profound). Fluorescence intensity values were calculated and analyzed using ImageJ. The high-K^+ stimulus contained the following (in mM): 85 NaCl, 70 KCl, 2.5 $CaCl_2$, 1 $MgCl_2$, 10 H-HEPES, and 10 D-glucose, pH 7.4, and was applied using a gravity perfusion system (RCP-2B, Yibo). In bafilomycin experiments, cells transfected with NPY-pHluorin were pretreated with 1 μM bafilomycin for 30 min and then TIRF imaging was performed as above.

TMR-dextran uptake. Cultured mouse ACCs were washed 3 times with standard extracellular bath solution and then incubated for 1 min with 50 μM dextran (10 and 40 kDa, Invitrogen, D1816 and D1842, respectively) in 70 mM K^+-containing external solution. Unbound dye was washed out with standard bath solution (without Ca^{2+}) immediately after incubation. *Z*-series of 1 μm optical sections were scanned through the 40× oil-immersion lens of a Zeiss 710 inverted confocal microscope. The consecutive optical sections were *z*-projected and the total numbers of dextran fluorescent puncta per cell were determined. Images were processed with ImageJ. All the above experiments were done at room temperature.

EM imaging. EM of adrenal slices was performed according to previous descriptions with minor modifications (de Wit et al., 2009a; Wang et al., 2016). The adrenal glands were extracted from adult WT and dyn1-KO mice and then the adrenal cortex was removed and the medulla was cut into 1–2 mm^3 pieces. These pieces were then immersed in 5% glutaral-

dehyde and 2% PFA in PBS for 1–2 h at room temperature. Cells were then postfixed for 30 min with 1% osmium tetroxide, washed, dehydrated through an ethanol series, embedded in Epon, and polymerized for 36 h at 60°C. Ultrathin sections (~80 nm) were collected on single-slot, Formvar-coated copper grids and stained with 2% uranyl acetate for 30 min and 0.5% lead citrate for 15 min. Samples were observed in a Tecnai G2 20 200 KV transmission electron microscope at 120 KV. Vesicle diameters and numbers were measured manually with the Zeiss LSM Image Browser (version 3.0) as described previously (Chen et al., 2008).

Western blot. Adrenal samples were washed with PBS and homogenized on ice with lysate buffer containing 20 mM HEPES at pH 7.4, 100 mM KCl, 2 mM EDTA, 1% NP-40, 1 mM PMSF, and 2% proteinase inhibitor (539134, Calbiochem). The homogenates were centrifuged at 16,000 × *g* for 15 min at 4°C and the supernatants were collected and boiled in SDS-PAGE buffer. Proteins were electrophoresed and transferred to nitrocellulose filter membranes. Each membrane was blocked by incubation for 1 h with PBS containing 0.1% Tween 20 (v/v) and 5% nonfat dried milk (w/v). After washing with 0.1% Tween 20 containing PBS (PBST), the blots were incubated with primary antibodies at 4°C overnight in PBST containing 2% bovine serum albumin (BSA). Secondary antibodies were then applied at room temperature for 1 h. Blots were scanned with an Odyssey infrared imaging system (LI-COR Biosciences) and quantified with ImageJ. The following primary antibodies were used: Dynamin 1 (PA1-660, Thermo Fisher Scientific), Dynamin 2 (ab3457, Abcam), VMAT1 (ab168347, Abcam), tyrosine hydroxylase (TH; AB152, Millipore), and actin (A5316, Sigma-Aldrich). The secondary antibodies were IRDye 800CW goat anti-rabbit IgG (LIC-926-32211, LI-COR Biosciences) and IRDye 680CW goat anti-mouse IgG (LIC-926-32220, LI-COR Biosciences).

Statistics. All experiments were replicated at least three times. Offline data analysis was performed using ImageJ and IGOR software (Wavemetrics). Data are presented as box-and-whisker plots or mean ± SEM. Box-and-whisker plots show medians (central line in the box), ranges between the 25th and 75th percentiles (box), and minimum–maximum ranges (whiskers). Statistical comparisons were performed using the two-tailed unpaired Student's *t* test and the Kolmogorov–Smirnov test for cumulative analysis. All tests were conducted using SPSS version 13.0. Significant differences were considered to be $p < 0.05$.

Results

dyn1 deficiency increases quantal size of catecholamine release

To verify dyn1-KO in mice, we found that the dyn1 protein was expressed in WT and successfully knocked out in ACCs from P3 mice (Fig. 1*H*; for details, see Ferguson et al., 2007). To evoke Ca^{2+}-dependent vesicle release in cultured ACCs, either caffeine (20 mM) or high KCl (70 mM) was used to increase intracellular Ca^{2+} ($[Ca^{2+}]_i$) via caffeine-sensitive Ca^{2+} stores or voltage-gated Ca^{2+} channels. When caffeine was applied for 5 s, a burst of amperometric spikes representing "quantal" catecholamine release from single LDCVs was evoked in both WT and KO cells (Fig. 1*A*,*B*). To analyze the kinetics of a quantal event, we defined the parameters foot duration, foot charge, peak amplitude (PA), half-height duration (HHD), and quantal size (QS) of single CFE spikes (Fig. 1*C*; see also Chen et al., 2005). Compared with the WT, the QS was significantly higher by 200 ± 38% in dyn1-KO cells (Fig. 1*D*,*E*). In addition, dyn1-KO also increased the PA, HHD, foot charge, and foot duration, whereas the release frequency remained unchanged (Fig. 1*E*). Importantly, among the top 10% of the largest quantal events in WT and KO cells, the QS was also dramatically higher by ~250% in dyn1-KO cells (Fig. 1*E*). To determine whether the vesicles are larger in dyn1-KO cells, we used EM imaging to visualize LDCVs in adrenal sections (Fig. 1*F*) and found that the vesicle size remained unchanged in dyn1-KO ACCs (Fig. 1*G*). Compared with previous EM images of neural vesicles, our EM results in ACCs are similar to those in the calyx of Held synapse (Lou et al., 2008), but different from those in hippocampal synapses with cluster-like vesicular structures or bulk-like structures (Raimondi et al., 2011; Ferguson and De Camilli, 2012). In addition, the expression levels of the vesicular catecholamine content-related proteins vesicular monoamine transporter 1 (VMAT-1) and TH also remained unchanged in KO ACCs (Fig. 1*I*), indicating that the increased quantal size of catecholamine release was not due to changes in vesicle size or catecholamine content per LDCV. Additional recordings of membrane capacitance revealed 50% smaller capacitance increases in WT versus KO cells (data not shown), consistent with the idea that KAR is the dominant release mode in WT cells. Collectively, these data suggest that all single-vesicle release events are subquantal in native ACCs.

dyn1 contains five functional domains (Fig. 1*J*), including the proline-rich domain that is involved in regulating QS in ACCs (Chen et al., 2005; Ferguson and De Camilli, 2012). In dyn1-KO cells, the phenotypes of increased QS and HHD were fully rescued by WT dyn1, but not dyn1-K44A, a dominant-negative GTPase mutation (Fig. 1*J*,*K*). In addition, the QS effect of dyn1-KO was not rescued by dyn2 (Fig. 2). dyn2 has a role in regulating slow endocytosis, but not dyn1-dependent fast endocytosis (Artalejo et al., 2002). We found that the expression of dyn2 was intact in dyn1-KO adrenal medulla (Fig. 2*D*) and its overexpression did not rescue QS in dyn1-KO ACCs (Fig. 2*A*–*C*). These experiments indicated the functional specificity of dyn1 in regulating fusion modes and fusion pore dilation. Therefore, the increased QS is specific to dyn1 deficiency and requires the GTPase activity of dyn1.

To further investigate the effect of dyn1 on QS under more physiological conditions, we did similar experiments in ACCs from adrenal slices (Fig. 3*A*,*B*) *versus* those in primary culture (Fig. 1). As in cultured ACCs, dyn1-KO also significantly increased the QS, PA, foot charge, and foot duration in adrenal slices stimulated by caffeine (Fig. 3*C*–*E*). Similar results were obtained in adrenal slices stimulated by 70 mM high-potassium (70 K) depolarization (Fig. 3*F*). The statistical data from slices (Fig. 3*E*,*F*) were consistent with those from cultured cells (Fig. 1*E*).

Together, the above data demonstrated that dyn1-KO increases QS, but does not affect the release frequency and vesicle size in ACCs in both the adrenal slice and primary culture.

Full-fusion events are increased by dyn1-KO

The above CFE recordings established that QS, but not release frequency, was increased by dyn1-KO. This raised the possibility that the release probability of full-quantal (or FFL) events could be increased by dyn1-KO. To test this prediction using a method independent of CFE recording, we used TIRF microscopy to monitor the dynamics of single exocytosis of pHluorin-tagged vesicle cargos in transfected ACCs (Fig. 4). The fluorescence of pHluorin is quenched as a result of the acidity of the vesicle lumen, but rapidly increases during opening of the fusion pore due to the deacidification effect of the neutral extracellular solution (Miesenböck et al., 1998). The mCherry protein is insensitive to pH changes, which permits monitoring of vesicles docking near the plasma membrane. In ACCs, the docked vesicles along the plasma membrane were similar in WT and dyn1-KO cells expressing NPY-mCherry (Fig. 4*A*). Based on the release and diffusion of fluorescent content measured by TIRF imaging, we distinguished two vesicle fusion modes, KAR and FFL (Fig. 4*A*–*F*; Movies 1 and 2; also see Perrais et al., 2004; Tsuboi et al., 2004;

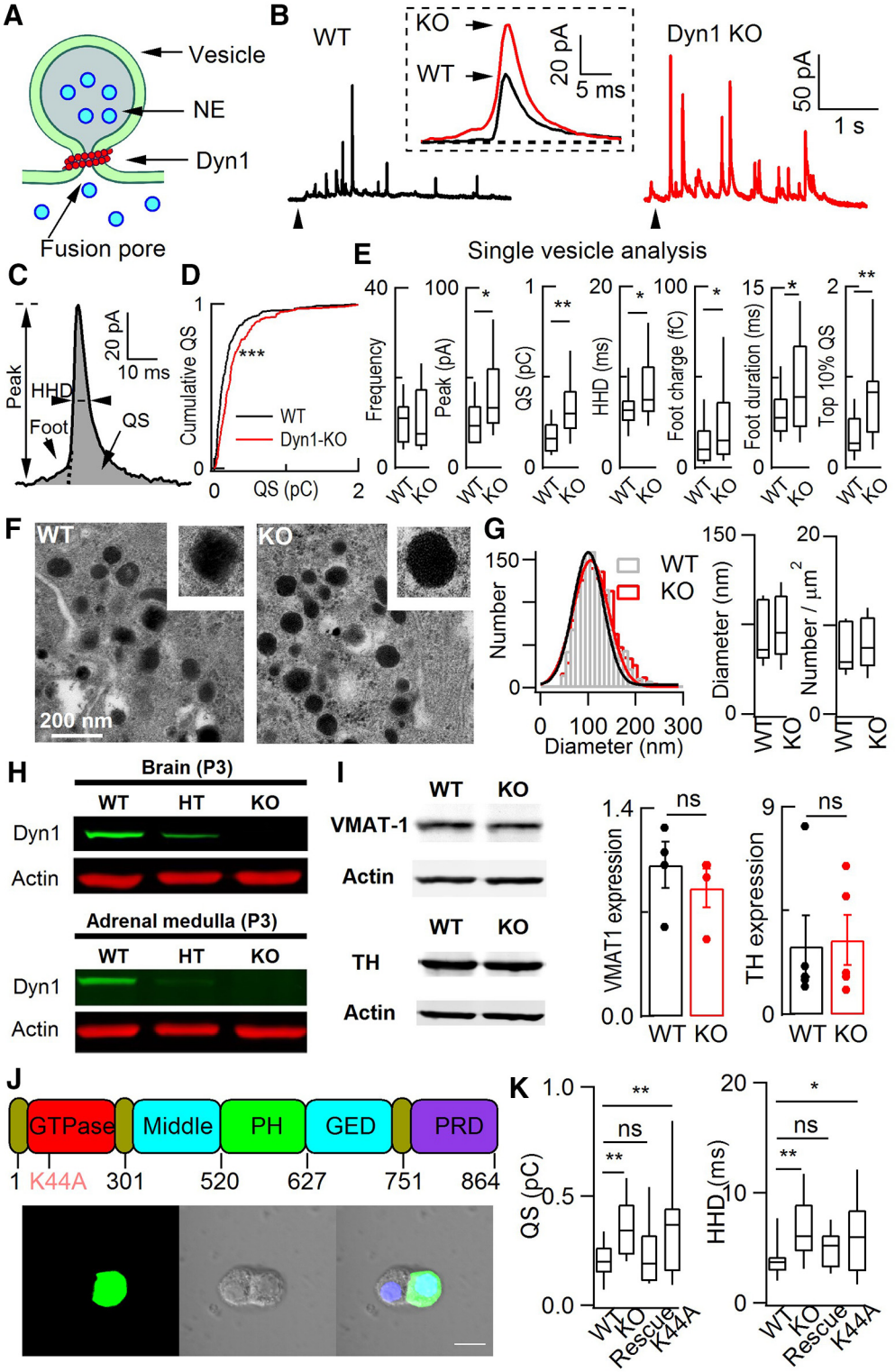

Figure 1. dyn1-KO increased quantal size in native ACCs. ***A***, Diagram depicting a fusion event between vesicle and plasma membrane, local catecholamine dyn1 and fusion pore. ***B***, Representative amperometric recordings of catecholamine release from WT and dyn1-KO ACCs evoked by 20 mM caffeine. Insert, Enlarged and averaged quantal events from WT and KO cells (each from 20 amperometric spikes among the fastest 10%, recorded from these two cells; Zhou et al., 1996). ***C***, Quantal event with defined parameters. ***D***, Cumulative analysis of QS in WT and dyn1-KO. Kolmogorov–Smirnov test, $p < 0.001$. ***E***, Quantitative analysis of single-vesicle release events (quanta). Analyzed spikes met the 5 SD threshold criterion (Chen et al., 2005). Data are from 18 cells and 162 quanta for WT, 15 cells and 224 quanta for KO. The median for quantal size increased from 0.13 pC (WT) to 0.25 pC (KO). Overlapping events that could not be separated from each other were removed from the statistics. ***F***, Representative EM images of sections from WT (left) and KO (right) cells. LDCVs are dispersed throughout the cytoplasm in both cell types. Scale bar, 200 nm. ***G***, Distribution and statistics of vesicle diameter and vesicle number per square micrometer. Left, Single Gaussian fitting of the distributions superimposed on the bar graphs [total of 1341 (WT, 15 cells) and 1414 vesicles (dyn1 KO, 16 cells)]. Right, Statistics of vesicle size and number per square micrometer for WT and dyn1-KO cells. ***H***, dyn1 expression and KO in brain and adrenal mudulla of P3 mice. dyn1-KO mice were killed and brain (positive control) and ACC tissues were isolated for Western blot. Representative images of three independent repeats are shown. HT, Heterozygous. ***I***, VMAT-1 and TH expression in adrenal medulla from WT and dyn1-KO mice. Four independent experiments were performed. For VMAT-1, from 6 WT littermates and 6 KO mice and 5 independent experiments; for TH, from 8 WT littermates and 8 KO mice. ***J***, Top, Diagram illustrating the functional domains of dyn1 and its GTPase dominant-negative mutation K44A. (*Figure legend continues.*)

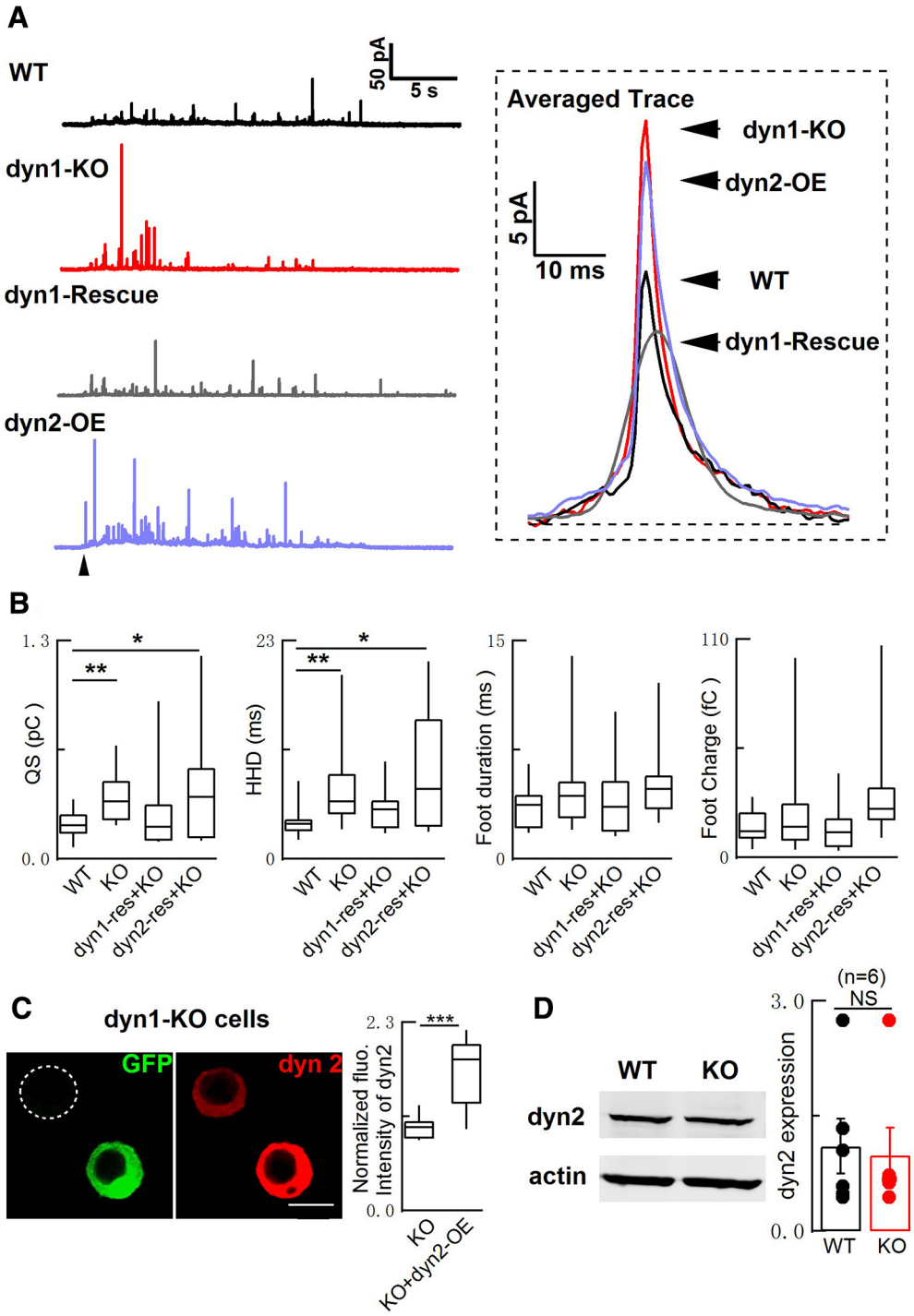

Figure 2. Overexpression of dyn2 failed to rescue the impaired quantal size in dyn1-KO cells. ***A***, Left, Representative CFE recordings from WT and dyn1-KO cells with or without dyn1-rescue or dyn2-rescue. Right, Averaged single spike events (17 quanta for WT; 25 for dyn1-KO; 42 for dyn1-rescue; and 42 for dyn2-rescue). ***B***, Statistics of QS, HHD, foot duration, and foot charge. WT: $n = 19$; KO: $n = 23$; Rescue: dyn1-KO cells rescued with WT-dyn1 ($n = 23$); dyn2: dyn1-KO cells rescued with dyn2 ($n = 14$); one-way ANOVA. ***C***, Immunofluorescence of dyn2 in dyn1-KO chromaffin cells transfected with GFP-tagged dyn2 plasmid for 48 h. The fluorescence intensity in cells overexpressing dyn2 (dyn2-OE) was normalized to native control cells ($n = 17$ cells for control and $n = 17$ cells for dyn2-OE, two-tailed unpaired Student's t test). Scale bars, 10 μm. ***D***, dyn2 expression in adrenal medulla from WT and dyn1-KO mice ($n = 6$ independent experiments, two-tailed unpaired Student's t test). Data are presented as median with interquartile range (***B***, ***C***) or mean ± SEM (***D***). NS for $p > 0.05$, $^{*}p < 0.05$, $^{**}p < 0.01$, $^{***}p < 0.001$.
←

(*Figure legend continued.*) Bottom, Two sister ACCs of the intact (left) and the dyn1 cell by transfected electroporation (right). Scale bar, 10 μm. ***K***, Statistics of dyn1 rescue. WT: $n = 19$; KO: $n = 23$; rescue: dyn1-KO was rescued by WT-dyn1 ($n = 23$); K44A: dyn1-KO was not rescued by dyn1-K44A ($n = 15$); one-way ANOVA. In all figures, animal numbers varied from three to five pairs of WT and KO littermates. Data are presented as medians with interquartile ranges (NS for $p > 0.05$, $^{*}p < 0.05$, $^{**}p < 0.01$, $^{***}p < 0.001$, two-tailed unpaired t test for ***E***, ***G***, and ***I***; one-way ANOVA for ***K***).

Bowser and Khakh, 2007; Matsuda et al., 2009; Xia et al., 2009; Zhang et al., 2009; Wang et al., 2017). As defined previously (Wang et al., 2017), KAR events showed a brief fluorescence increase in the center, but without a clear fluorescence increase in the annular area (Fig. 4*C*,*D*), representing a transient opening and reclosure of a restricted fusion pore. Conversely, FFL events showed a robust fluorescence increase occurring at

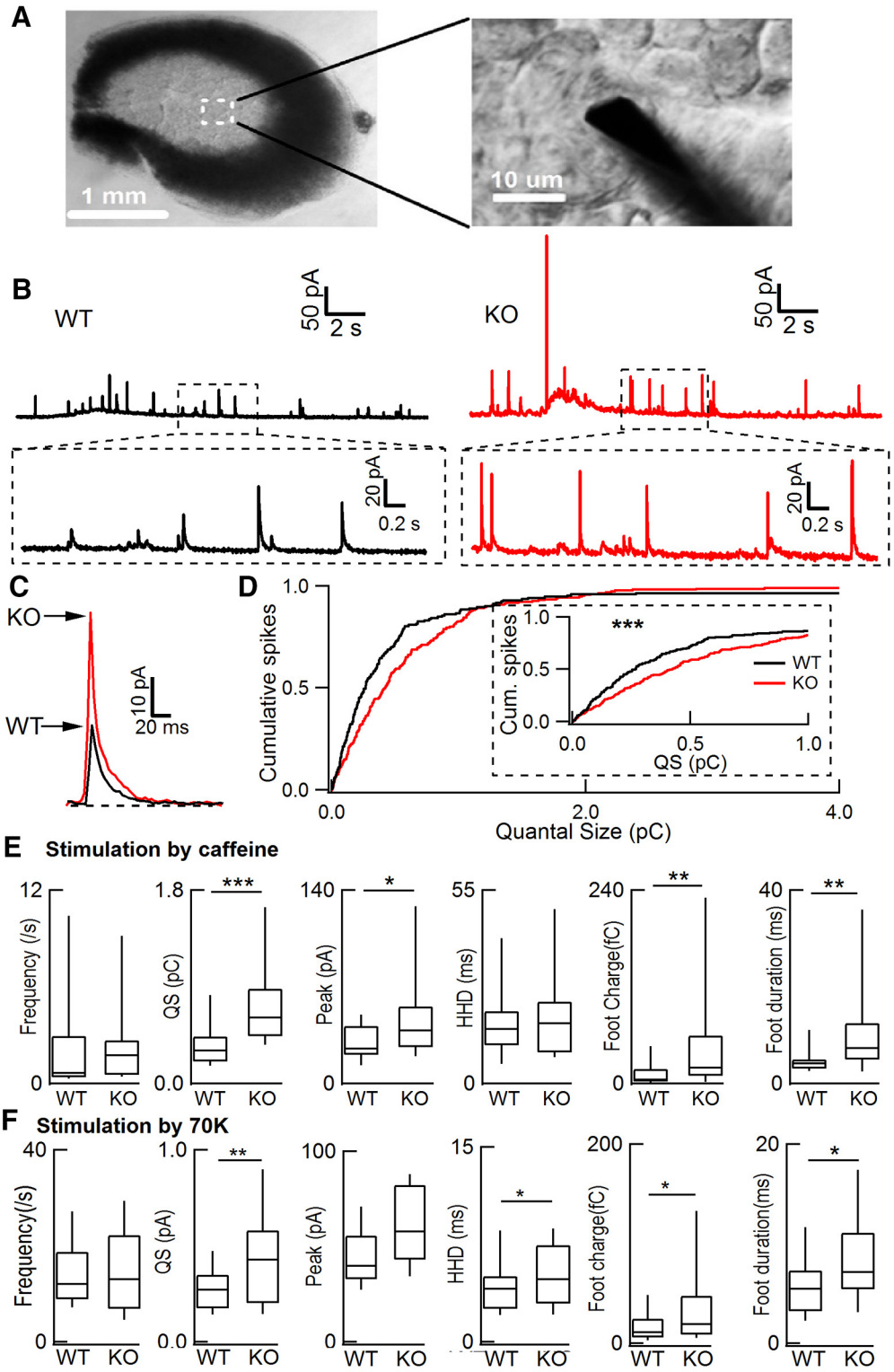

Figure 3. dyn1-KO increased quantal size in adrenal slice cells. ***A***, Image of a freshly prepared mouse adrenal slice 150 μm thick. Inset, Enlargement containing a recording CFE (Φ7 μm) in the slice with visible individual ACCs. ***B***, Representative amperometric recordings of quantal catecholamine release in ACCs from adrenal slices exposed to 50 mM caffeine for 20 s. ***C***, Averaged quantal traces (29 events from a WT cell and 22 events from a KO cell) from ***B***. ***D***, Cumulative analysis of QS in WT and dyn1-KO. Inset, Enlarged cumulative traces. Kolmogorov–Smirnov test, $p < 0.001$. ***E***, Statistics of frequency, QS, peak, HHD, foot charge, and foot duration ($n = 13$ WT cells from 4 WT mice, $n = 24$ KO cells from 6 KO littermates, stimulated by caffeine). ***F***, Statistics of frequency, QS, peak, HHD, foot charge and foot duration ($n = 15$ WT cells from 3 WT mice, $n = 17$ KO cells from 3 KO littermates, stimulated by 70 K depolarization). Data are presented as median with interquartile range. *$p < 0.05$, **$p < 0.01$, ***$p < 0.001$, two-tailed unpaired *t* test.

both the center and the annular area of NPY-pHluorin puncta (Fig. 4*E*,*F*), implying that the fusion pore was large enough for full cargo release. The detailed parameters used to definite the KAR and FFL events are described in the Materials and Methods.

The modes of KAR and FFL determined by TIRF imaging in Figure 4 were based on following evidence: (1) the membrane-to-coverslip distance was stable over a large continuous area (see Movies 1, 2, 3 and 4); (2) the events were spatially and tem-

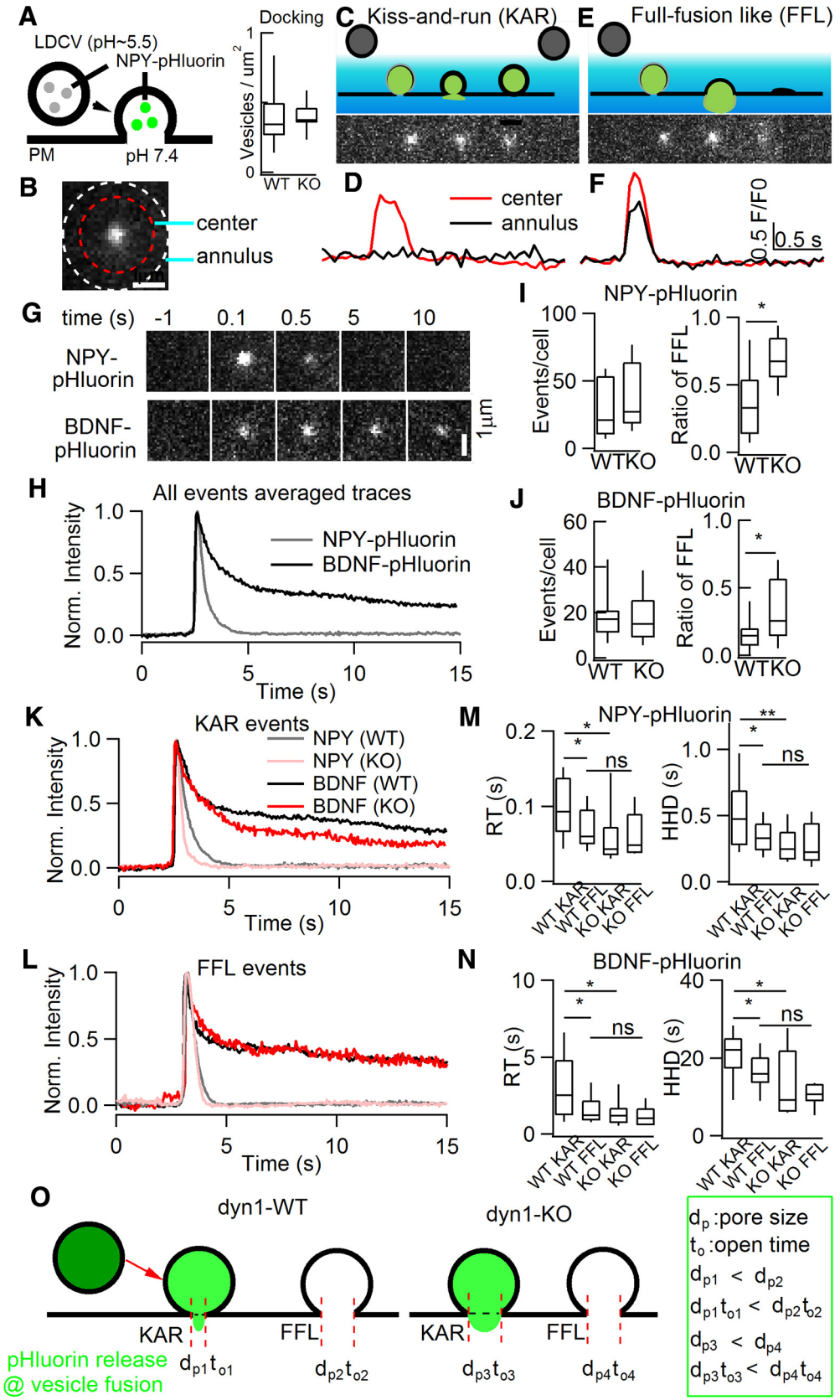

Figure 4. "Full-fusion-like" release probability and d_p were substantially increased as revealed by live imaging of single-vesicle release. ***A***, Left, Diagram depicting the pH dependence of NPY-pHluorin. Right, dyn1-KO did not affect vesicles docking by using NPY-mcherry. ***B***, Regarding the center and annulus in TIRF image of NPY-pHluorin release events, followed previous criteria and definitions (Bowser and Khakh, 2007; Wang et al., 2017), representative areas selected for fluorescence calculation: center diameter, 1.92 μm; annulus, 2.4 μm. ***C***–***F***, Definitions of two release modes, KAR (***C***) and FFL (***E***). ***D***, ***F***, Representative fluorescence intensity of KAR (***D***) and FFL (***F***). Note that, compared with FFL, KAR events showed only a brief brightening of the release center, but little fluorescence increase in the annular area. Red, Center fluorescence intensity; black, annulus intensity. ***G***, ***H***, Representative time-lapse (***G***) and normalized fluorescence intensity (***H***) of NPY-pHluorin and BDNF-pHluorin events. TIRF image frames, 2.4 μm × 2.4 μm; cell numbers, 34 for NPY-pHluorin, 32 for BDNF-pHluorin; animal numbers, (*Figure legend continues.*)

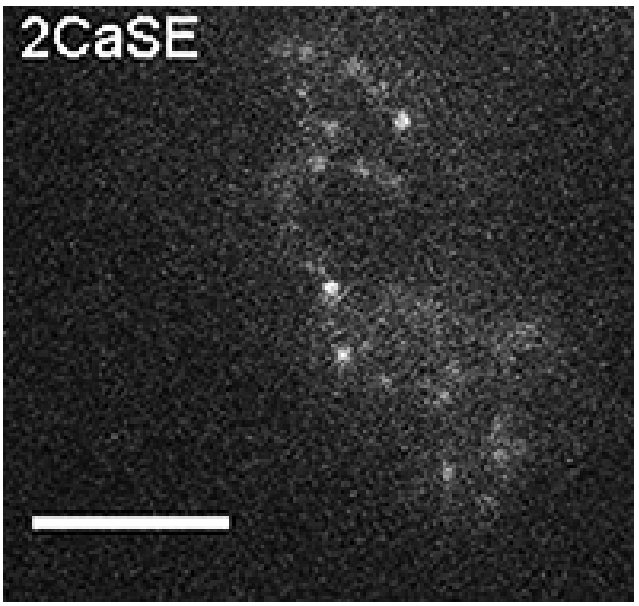

Movie 1. Real-time imaging of NPY-pHluorin release in a dyn-WT ACC by TIRF microscopy. The movie show simultaneous imaging of NPY-pHluorin release from individual vesicles in a WT stimulated by KCl (70 mM) depolarization. The cell was from littermates of Movie 2. Scale bar, 5 μm.

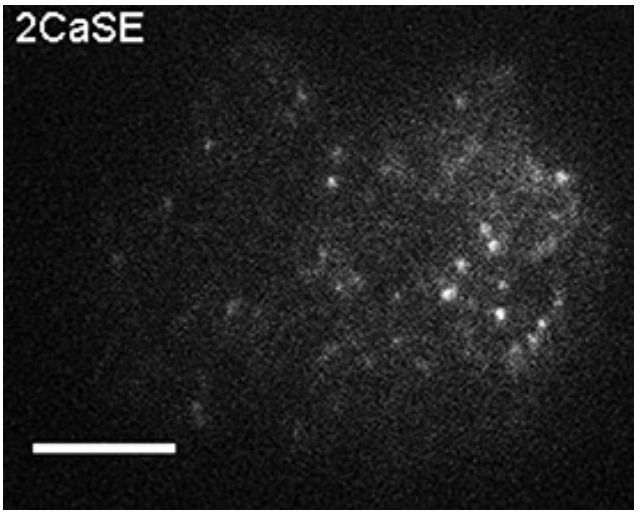

Movie 2. Real-time imaging of NPY-pHluorin release in a dyn1-KO ACC by TIRF microscopy. The movie show simultaneous imaging of NPY-pHluorin release from individual vesicles in dyn1-KO ACC stimulated by KCl (70 mM) depolarization. The cell was from littermates of Movie 1. Scale bar, 5 μm.

←

(*Figure legend continued.*) 8 pairs of WT and KO. ***I***, ***J***, Statistics of number of events per cell (left) and ratio of "full-fusion-like, FFL" (right) for NPY-pHluorin and BDNF-pHluorin release. ***K***, ***L***, Normalized fluorescence intensity of KAR (***K***) and FFL (***L***) events. ***M***, ***N***, Statistics of RT and HHD of NPY-pHluorin (***M***) and BDNF-pHluorin (***N***) events (NPY-pHluorin: $n = 15$ WT cells and total 232 events for KAR, 128 events for FFL; $n = 19$ KO cells and total 182 events for KAR, 253 events for FFL. BDNF-pHluorin: $n = 18$ WT cells and 161 events for KAR, 68 events for FFL; $n = 14$ KO cells and 183 events for KAR, 91 events for FFL; one-way ANOVA). ***O***, Diagram illustrating results from ***K***–***N***. KAR versus FFL in WT and dyn1-KO are jointly determined by fusion pore open time (t_o) and d_p. Data are presented as median with interquartile range (ns for $p > 0.05$, $^*p < 0.05$, $^{**}p < 0.01$, $^{***}p < 0.001$, two-tailed unpaired *t* test for ***I*** and ***J***, one-way ANOVA for ***M*** and ***N***).

porally random (see Movies 1, 2, 3 and 4; also see Duncan et al., 2003; Perrais et al., 2004), similar to that in astrocytes (Bowser and Khakh, 2007) and sensory neurons (Wang et al., 2017); (3) FFL events were increased in KO versus WT cells (Fig. 4*I*); (4) the number of docking vesicles was similar in KO and WT cells (Fig. 4*A*); (5) as revealed by NH_4Cl quench of pHluorin (data not shown), the pHluorin decay signal reflects the transient opening-closing of the fusion pore in both WT and KO cells; and (6) similar results for KAR and FFL are fully consistent with CFE amperometry (Figs. 1, 2, 3), blockade of proton pump by bafilomycin (see below), as well as dextran uptake (see below).

We also investigated whether dyn1-KO affects single-vesicle release using TIRF imaging. Strikingly, dyn1-KO increased the FFL event ratio from 25 ± 6% to >70% of the total LDCV fusion events evoked by KCl depolarization, whereas the release frequency remained unchanged (Fig. 4*I*). Next, we analyzed the release kinetics of single fusion events in WT and dyn1-KO ACCs (Fig. 4*K*–*N*). Averaging all KAR events (Fig. 4*K*) showed that dyn1-KO dramatically reduced the rise time (RT) and HHD (Fig. 4*M*), indicating that dyn1 decreases the fusion pore size (d_p) and decelerates release, so events are faster in the KO than in the WT (Fig. 4*O*). In dyn1-WT cells, there was a notable difference between KAR and FFL events. Both RT and HHD of a quantal spike were substantially slower during KAR (RT ~100 ms, HHD ~470 ms) versus FFL (RT ~70 ms, HHD ~300 ms). In KO cells, surprisingly, these kinetic differences between KAR and FFL events were abolished (Fig. 4*M*). The longer RT of KAR was probably due to the smaller fusion pore and the fact that the vesicular H^+ pump balanced a higher percentage of H^+ influx, leading to slower quenching of pHluorin at KAR in WT cells. The HHD of quantal events determined in Figure 1*E* by CFE and in Figure 4,*M* and *N*, by TIRF were opposite. This was probably because that HHD in Figure 1*E* represents the released catecholamine from the vesicles, whereas HHD in Figure 4, *M* and *N*, represents the remained contents (NPY-pHluorin) after vesicle release. Because more contents were released in dyn1-KO cells (see below), the decay was faster in dyn1-KO (Fig. 4*M*,*N*).

Because dyn1 slows the vesicle content release in WT cells (Fig. 4*M*,*N*), more content may remain in vesicles after fusion. To test this hypothesis, we pretreated cells with 1 μM bafilomycin (a vesicular H^+-ATPase inhibitor; Zhu et al., 2009), for 30 min to inhibit the reacidification of pHluorin and to detect the remaining content after KAR release (Fig. 5). Compared with results such as those shown in Figure 4*M* without bafilomycin treatment, we found that bafilomycin treatment significantly increased the RT and HHD of WT KAR events, but had minor effects on the HHD and RT of KO events (Fig. 5*B*–*D* and Movies 3 and 4), indicating that dyn1 constricted the release kinetics of contents from the fusion pore. Therefore, more fluorescent cargo was retained in WT versus KO cells and was released in a slower pattern (Fig. 5).

Because the release of NPY-pHluorin (monomer ~30 kDa) was sufficiently rapid to challenge the capture rate of our TIRF microscope (20 Hz, or 50 ms per image), we also examined the larger vesicular cargo BDNF-pHluorin (dimer ~2 × 45 kDa). Consistent with NPY-pHluorin, dyn1-KO increased the percentage of FFL release events of BDNF-pHluorin (Fig. 4*J*), but with a longer discharge time than NPY-pHluorin (Fig. 4*G*,*H*). This BDNF-pHluorin dynamics was similar to the previous report of a slower pattern in both exocytosis and endocytosis (Aoki et al., 2010). It is known that mature BDNFs dimerize (Xia et al., 2009) and interact with other luminal components (de Wit et al., 2009b), which leads to an unbinding process and probably causes the distinct biphasic decay (Fig. 4*G*,*H*). Although the RT of NPY-

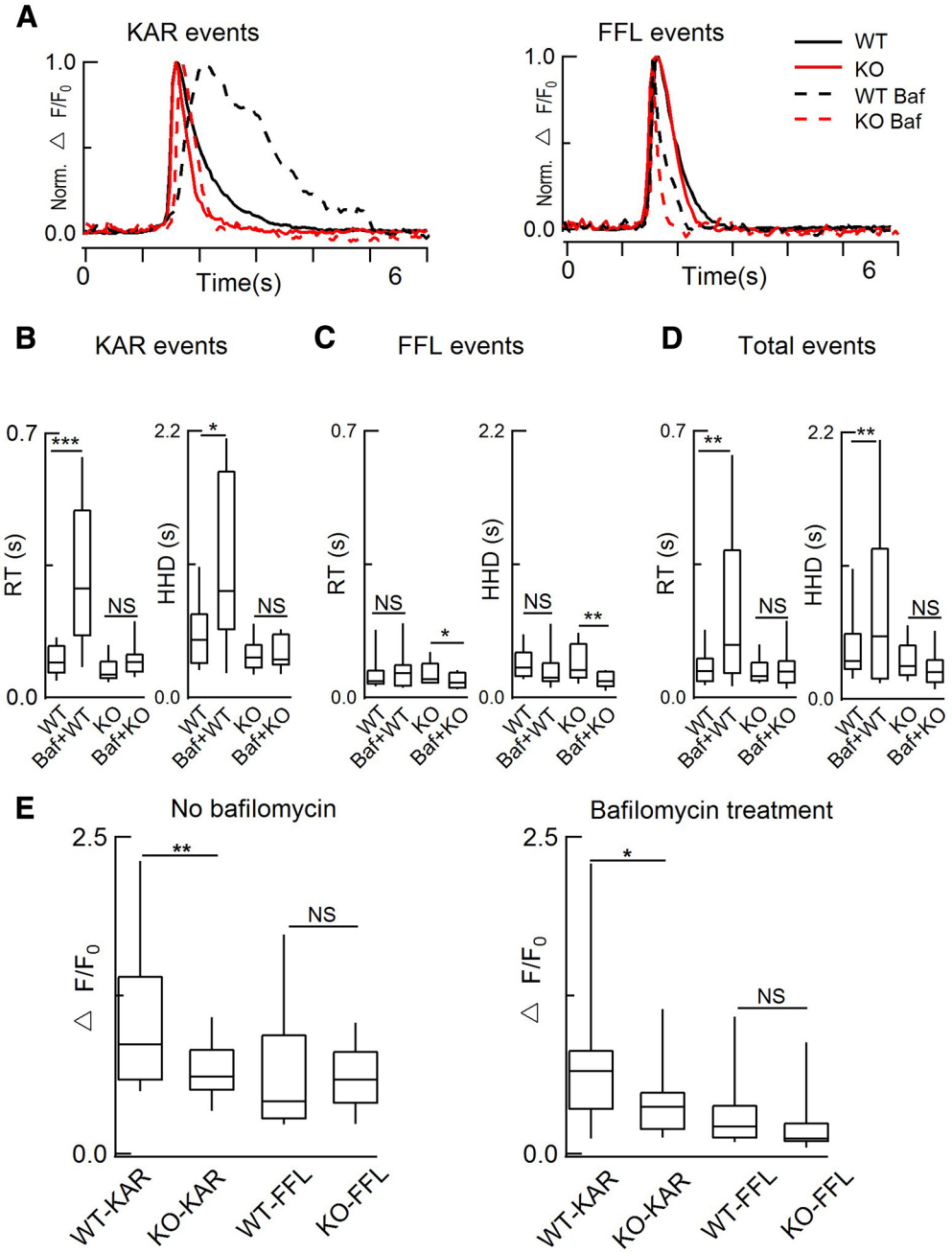

Figure 5. Bafilomycin treatment selectively slowed the release kinetics in WT versus dyn1-KO cells. ***A***, Normalized NPY-pHluorin fluorescence intensity of KAR events (left, see Fig. 4*D*) and FFL events (right, see Fig. 4*F*) with and without 1 μM bafilomycin (Baf) pretreatment for 30 min in WT and dyn1-KO ACCs. ***B–D***, Statistics of ***A***. As shown in ***D***, bafilomycin significantly increased the RT and HHD of WT versus KO events (without Baf: total 232 KAR events and 128 FFL events from $n = 15$ WT cells; 182 KAR events and 253 FFL events from $n = 19$ KO cells, 8 pairs of WT and KO littermates; with Baf: 245 KAR events and 60 FFL events from $n = 13$ WT cells; 214 KAR events and 71 FFL events from $n = 11$ KO cells, 10 WT and 8 KO littermates). ***E***, Vesicle fluorescence intensity ($\Delta F/F_0$) was larger in WT versus KO cells. In KAR events, the $\Delta F/F_0$ was significantly larger in WT versus KO events in cells either without bafilomycin treatment (**$p < 0.01$), $n = 15$ (WT) and 19 (KO) cells from 8 WT and 8 KO littermates or with bafilomycin treatment (*$p < 0.05$), $n = 13$ (WT) and 11 (KO) cells from 10 WT and 8 KO littermates. Data are presented as median with interquartile range (NS for $p > 0.05$, *$p < 0.05$, **$p < 0.01$, ***$p < 0.001$, one-way ANOVA).

PHluorin (but not BDNF-pHluorin) was close to the limit of the TIRF sample rate (20 Hz or 50 ms), the statistical averaging of RT and HHD increased the temporal resolution beyond the TIRF sample rate, as evident by the similar results using either NPY-pHluorin or BDNF-pHluorin (Fig. 4). Therefore, either of these indicators is suitable for studying dyn1-KO effects in ACCs (Fig. 4*K*,*N*).

Together, these data strongly suggest the following: (1) the WT-d_p of FFL events is as large as that of KO (both KAR and FFL) events to release most (or all) of the NPY-pHluorin during an exocytotic event (Fig. 4*K*,*M*); (2) KAR events in KO cells (<30% of total events, Fig. 4*I*) have a larger fusion pore (Fig. 4*M*) and a shorter open time; and (3) dyn1 is not required for vesicle fusion, but is an essential factor to restrict d_p size during fusion (Fig. 4*M*). These single-vesicle imaging data lead to the conclusion that dyn1 maintains vesicles in the KAR mode, most likely by reducing the d_p (Fig. 4*O*).

dyn1-KO increases d_p as determined by endocytosis assay

We used another independent fluorescence-based method to estimate the expansion of the fusion pore in WT and dyn1-KO

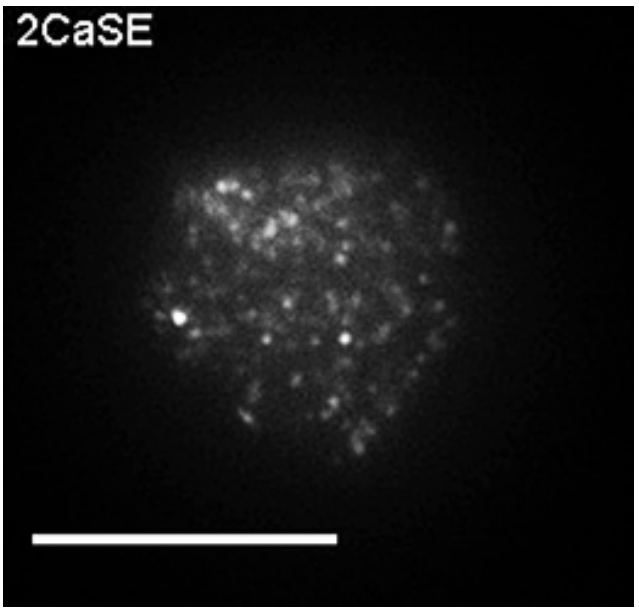

Movie 3. Real-time imaging of NPY-pHluorin release in a dyn-WT ACC (pretreated with 1 μM bafilomycin) by TIRF microscopy. The movie show simultaneous imaging of NPY-pHluorin release from individual vesicles in WT (Movie 3) and dyn1-KO ACC (Movie 4) stimulated by KCl (70 mM) depolarization. Before imaging, ACCs were treated with 1 μm bafilomycin for 30 min. The cell was from littermates of Movie 4. Scale bar, 10 μm.

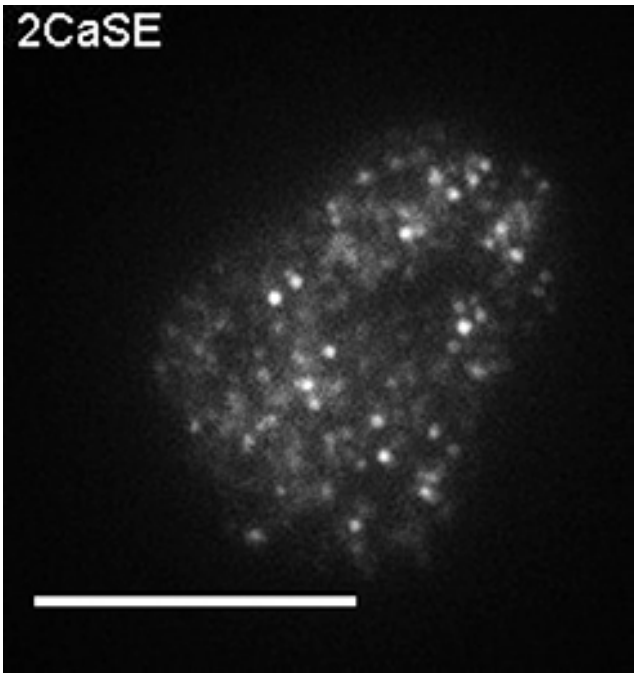

Movie 4. Real-time imaging of NPY-pHluorin release in a dyn1-KO ACC (pretreated with 1 μM bafilomycin) by TIRF microscopy. The movie show simultaneous imaging of NPY-pHluorin release from individual vesicles in WT (Movie 3) and dyn1-KO ACC (Movie 4) stimulated by KCl (70 mM) depolarization. Before imaging, ACCs were treated with 1 μm bafilomycin for 30 min. The cell was from littermates of Movie 3. Scale bar, 10 μm.

ACCs. Fluorescence-tagged dextran is a large inert fluid-phase marker and has been used as nanoparticles to estimate d_p during the exocytosis–endocytosis process (Fulop et al., 2005; Clayton et al., 2008; Raghupathi et al., 2016). ACCs were loaded with different-sized dextrans dissolved in high K^+ and then unbound dye was immediately washed out with standard bath solution (without Ca^{2+}). Cells were then scanned in *Z*-stacks by confocal imaging. With small dextran (10 kDa, Φ 5 nm), dextran uptake into vesicles was similar in KO and WT cells (Fig. 6*A*,*C*). However, the uptake of larger dextran (40 kDa, Φ 9 nm) was significantly greater in KO cells than in WT cells (Fig. 6*B*,*D*) and this phenomenon also occurred in cells without K^+ stimulation (Fig. 6*E*,*F*). Together, these data imply that, in addition to dextran uptake by endocytosis fission, at least part of the dextran uptake is due to influx of dextran through the KAR fusion pore, the size of which (d_p) was increased from 5 nm $< d_p <$ 9 nm to $d_p >$ 9 nm by dyn1-KO (Fig. 6*G*).

Independently, somatostatin, which activates GPCR-Gi-$\beta\gamma$ and reduces QS (Chen et al., 2005), inhibited the uptake of large (40 kDa), but not small (10 kDa), dextran, supporting the assumption that d_p can be estimated by the uptake of dextran nanoparticles into ACCs (data not shown).

Discussion

In neuroscience, the classic neurotransmission hypothesis is that Ca^{2+}-dependent vesicular neurotransmitter release occurs via "all-or-none" quanta. This dogma has been challenged by evidence that subquantal "stand-alone-foot" (mediated by KAR vesicle fusion) release exists in neuroendocrine ACCs (Zhou et al., 1996; Albillos et al., 1997) and in synaptic terminals (Stevens and Williams, 2000; He and Wu, 2007; Alabi and Tsien, 2013). It is unclear, however, how much subquantal release affects total catecholamine release in ACCs. In this work, we demonstrated that dyn1 maintains most (if not all) vesicular catecholamine release via the subquantal KAR ($\leq$40% of content per exocytotic event) mode in ACCs, as supported by four distinct fusion-pore assays (CFE, TIRF-pHluorin, bafilomycin-quenching, and dextran uptake). dyn1 restricts the fusion pore during vesicle fusion with the plasma membrane (Fig. 6*G*).

One major finding of this work was that, following Ca^{2+} influx, dyn1 caused most exocytotic vesicles to release catecholamine as subquantal events in WT ACCs. This is supported by the following evidence from cultured ACCs: (1) physiologically, we have previously reported that QS is reduced by endogenous ATP via GPCR-Gi-$\beta\gamma$, indicating the existence of subquantal release in ACCs (Chen et al., 2005); (2–3) pharmacologically, the QS of evoked release events was increased either (2) by acute application of a protein kinase C agonist or (3) by whole-cell dialysis of the proline-rich domain of dyn1, implying that part of the previously assumed quanta might be subquantal (Chen et al., 2005); (4–5) genetically, dyn1-KO increased the largest QS of evoked events by 250% (Fig. 1*A*–*E*), whereas the (4) vesicle size and (5) vesicle contents remained unchanged (Fig. 1*F*,*G*,*I*); and (6) dyn1-KO also increased the QS in fresh adrenal slices (Fig. 3). Together, these data established that dyn1-KO increases the largest single release events by 250%. Therefore, most (if not all) Ca^{2+}-evoked vesicle release events are subquantal.

Our second major finding was the mechanism by which dynamin produces subquantal release. We found that dyn1-KO increases QS by increasing the d_p. This is supported by the following evidence from comparison of KO and WT cells: (1) the increased QS was fully rescued by transfecting dyn1-WT but not GTPase-deficient (dominant-negative mutation dyn1-K44A) (Fig. 1*J*,*K*) or dyn2-WT (Fig. 2) into ACCs; (2) TIRF imaging of single-vesicle NPY-release showed that dyn1-KO increased the ratio of FFL to KAR events (Fig. 4*A*–*I*); (3) the temporal kinetics was faster in FFL than KAR in WT cells, but not KO cells, indi-

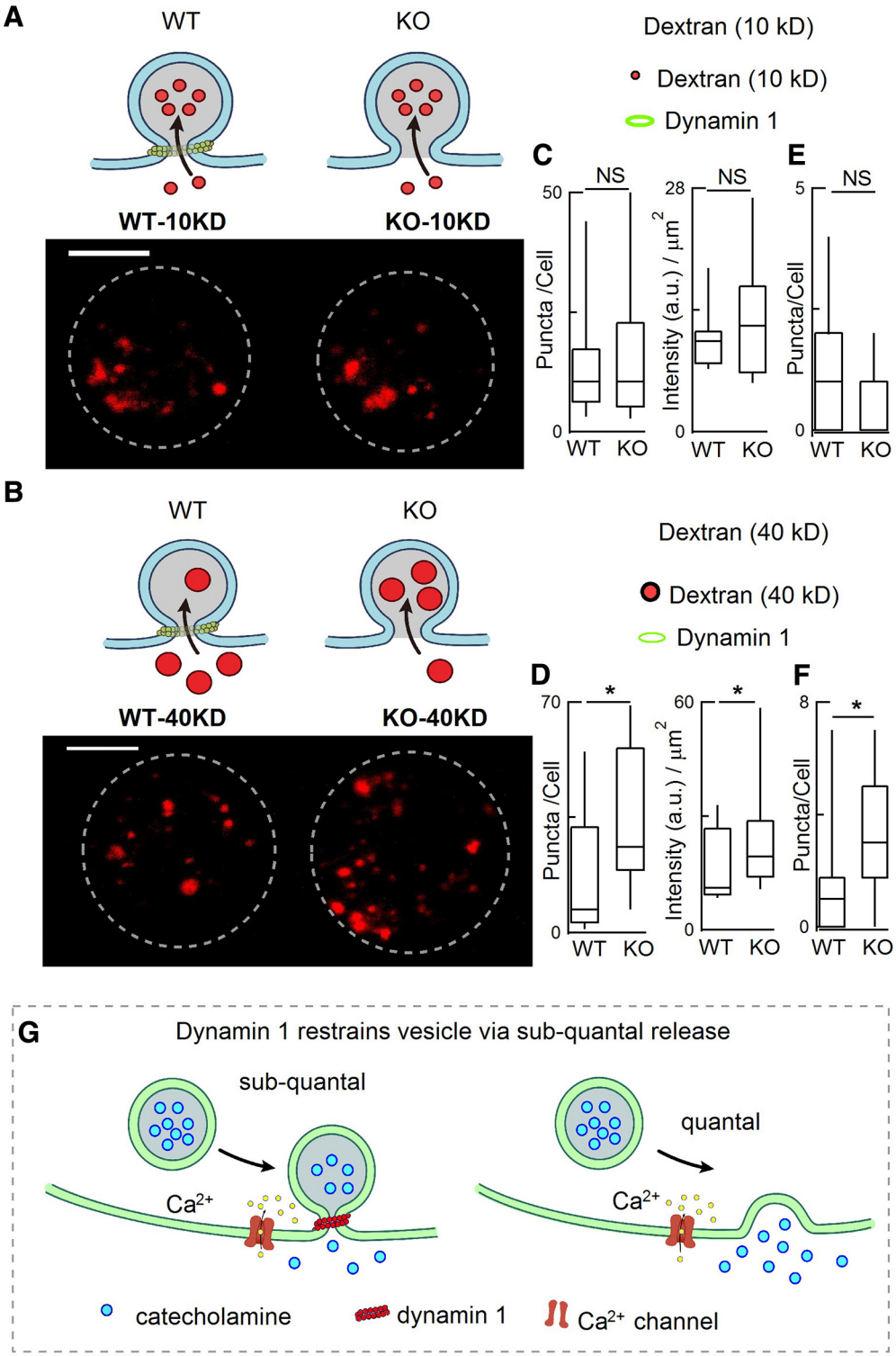

Figure 6. dyn1-KO increased the endocytic uptake of large dextran nanoparticles. ***A***, ***B***, Diagrams (top) and representative images (bottom) showing the uptake of TMR-dextran during 70 mM KCl stimulation for 1 min. Diagrams (***A***) show that small (10 kD) TMR-dextran was easily taken up by both WT and KO cells, whereas large (40 kD) TMR-dextran was more selectively taken up by KO cells (***B***). ***C***, ***D***, statistics of TMR-dextran number/cell and intensity/square micrometer [10 kDa TMR-dextran Φ 5 nm, 40 kDa TMR-dextran $\Phi \sim 9$ nm; 19 WT-cells (10 kDa), 19 WT-cells (40 kDa), 16 KO-cells (10 kDa), 19 KO-cells (40 kDa)]. Cells were from the same 4 WT mice and 4 KO littermates. Scale bar, 5 μm. ***E***, ***F***, Statistics of 10 KD TMR-dextran puncta taken up by WT ($n = 9$ cells) and dyn1-KO cells ($n = 12$ cells) without K^+ stimulation (***E***); statistics of 40 KD TMR-dextran puncta taken up by WT ($n = 16$ cells) and dyn1-KO cells ($n = 18$ cells) without K^+ stimulation (***F***), the large (40 KD) TMR-dextran was more selectively taken up by KO than by WT cells. Cells were from littermates (3 WT and 3 KO). Data are presented as median with interquartile range, $^*p < 0.05$, two-tailed unpaired *t* test. ***G***, Model of fusion pore and release modes regulated by dyn1. Left, Diagram depicting vesicle fusion with the plasma membrane while the fusion pore expansion is restricted by dyn1, resulting in subquantal release (KAR). Right, in the absence of dynamin 1, the fusion pore expands more, resulting in full-quantal release ("full-fusion"). Data are presented as median with interquartile range (NS for $p > 0.05$, $^*p < 0.05$, two-tailed unpaired *t* test).

cating that KO led to a d_p as large as FFL (Fig. 4*M*,*N*); (4) more vesicle content was retained after release in WT cells (Fig. 5); (5) dyn1-KO increased the d_p from <9 nm (range 5–9 nm) to >9 nm, as revealed by the uptake of nanoparticle dextrans (Fig. 6); and (6), importantly, the EM-based vesicle size and the expression of VMAT1 and TH did not differ between KO and WT cells (Fig. 1*F*,*G*,*I*). Together, these data demonstrated that dyn1 maintains most of the Ca^{2+}-induced exocytosis as subquantal release by restricting the d_p to <9 nm in native WT ACC cells.

In a previous study, dysbindin, a schizophrenia susceptibility protein, was found to regulate QS in both ACCs and hippocampal synapses (Chen et al., 2008). However, its regulatory pathway must be different from that of dyn1 because vesicle sizes are increased in dysbindin-KO cells but not in dyn1-KO cells (Fig. 1*F*,*G*). Although a caveat of off-target effects must always be considered with pharmacological methods, previous studies have reported evidence for the involvement of dynamin in QS (Chen et al., 2005; González-Jamett et al., 2010, 2013; Jackson et al., 2015). Anantharam et al. reported that overexpression of dyn1-GTPase mutations modulates fusion pore flickering (Anantharam et al., 2011). Only in a small number of vesicles did exocytosis colocalize with dyn1 during and after vesicle fusion. In the present work, however, even the top 10% of the largest release events was regulated by dyn1, suggesting that all release events are subquantal. In addition, dual color TIRFM imaging of dyn1 and NPY-pHluorin revealed >50% of KAR events with dyn1 accumulated at the fusion site (data not shown). One possibility for the difference could be that we used dyn-KO versus their transfection using Ca^{2+} phosphate. Based on single vesicle exocytosis of NPY-GFP imaged by TIRF in chromaffin cells, Almers et al. have proposed that, in 20% of exocytotic events, the cargo proteins (including NPY-GFP) are retained in the vesicle after resealing the fusion pore (Perrais et al., 2004). However, they assumed that catecholamine release is full quantal in all events (Perrais et al., 2004).

dyn1 is widely expressed in all neuronal cells (Ferguson et al., 2007; Ferguson and De Camilli, 2012) and increases vesicle size in EM and peak amplitude of mEPSC and mIPSC dyn1-KO synapse in physiological recordings (Ferguson et al., 2007; Lou et al., 2008; Raimondi et al., 2011). dyn1-KO revealed that probably all previously assumed "quantal release" are subquantal in chromaffin cells (Figs. 1, 2, 3). Future works should determine the following: (1) whether dyn1 produces also subquantal release in synapses via small clear vesicles and (2) in other cells containing LDCVs; (3) why are the dynamics similar during a KAR versus FFL release in KO cells (Fig. 4*K*–*O*)?; (4) whether/how other KAR proteins such as GPCR-Gi-$\beta\gamma$, synaptophysin, and syndapin (Chen et al., 2005; González-Jamett et al., 2010; Samasilp et al., 2012) work together with dyn1 to regulate KAR; and (5) how much (as a percentage) exocytosis is there in chromaffin cells (40% is an upper limit, Fig. 1*E*); and (6) what is the diversity between dyn2 in pancreatic β cells (Fan et al., 2015) and dyn1 in ACCs (Fig. 2).

The present study provides compelling evidence that most (if not all) Ca^{2+}-induced exocytosis events occur via the subquantal mode to release catecholamine content (≤40%) in ACCs. dyn1 induces subquantal KAR release mode by restricting the d_p so that ≥60% of catecholamine cannot be released before the fusion pore recloses. Our work provides an example from chromaffin cells, where Bernard Katz's hypothesis of Ca^{2+}-dependent transmitter release is revised from the "all-or-none/quantal" to the "subquantal" mode, implying that subquantal release could also exist in other secretion areas including neurotransmissions.

References

Alabi AA, Tsien RW (2013) Perspectives on kiss-and-run: role in exocytosis, endocytosis, and neurotransmission. Annu Rev Physiol 75:393–422. CrossRef Medline

Albillos A, Dernick G, Horstmann H, Almers W, Alvarez de Toledo G, Lindau M (1997) The exocytotic event in chromaffin cells revealed by patch amperometry. Nature 389:509–512. CrossRef Medline

Alés E, Tabares L, Poyato JM, Valero V, Lindau M, Alvarez de Toledo G (1999) High calcium concentrations shift the mode of exocytosis to the kiss-and-run mechanism. Nat Cell Biol 1:40–44. CrossRef Medline

Alvarez de Toledo G, Fernández-Chacon R, Fernández JM (1993) Release of secretory products during transient vesicle fusion. Nature 363:554–558. CrossRef Medline

Anantharam A, Bittner MA, Aikman RL, Stuenkel EL, Schmid SL, Axelrod D, Holz RW (2011) A new role for the dynamin GTPase in the regulation of fusion pore expansion. Mol Biol Cell 22:1907–1918. CrossRef Medline

Aoki R, Kitaguchi T, Oya M, Yanagihara Y, Sato M, Miyawaki A, Tsuboi T (2010) Duration of fusion pore opening and the amount of hormone released are regulated by myosin II during kiss-and-run exocytosis. Biochem J 429:497–504. CrossRef Medline

Artalejo CR, Elhamdani A, Palfrey HC (2002) Sustained stimulation shifts the mechanism of endocytosis from dynamin-1-dependent rapid endocytosis to clathrin- and dynamin-2-mediated slow endocytosis in chromaffin cells. Proc Natl Acad Sci U S A 99:6358–6363. CrossRef Medline

Bowser DN, Khakh BS (2007) Two forms of single-vesicle astrocyte exocytosis imaged with total internal reflection fluorescence microscopy. Proc Natl Acad Sci U S A 104:4212–4217. CrossRef Medline

Chen XK, Wang LC, Zhou Y, Cai Q, Prakriya M, Duan KL, Sheng ZH, Lingle C, Zhou Z (2005) Activation of GPCRs modulates quantal size in chromaffin cells through G(betagamma) and PKC. Nat Neurosci 8:1160–1168. CrossRef Medline

Chen XW, Feng YQ, Hao CJ, Guo XL, He X, Zhou ZY, Guo N, Huang HP, Xiong W, Zheng H, Zuo PL, Zhang CX, Li W, Zhou Z (2008) DTNBP1, a schizophrenia susceptibility gene, affects kinetics of transmitter release. J Cell Biol 181:791–801. CrossRef Medline

Chow RH, von Rüden L, Neher E (1992) Delay in vesicle fusion revealed by electrochemical monitoring of single secretory events in adrenal chromaffin cells. Nature 356:60–63. CrossRef Medline

Clayton EL, Evans GJ, Cousin MA (2008) Bulk synaptic vesicle endocytosis is rapidly triggered during strong stimulation. J Neurosci 28:6627–6632. CrossRef Medline

Crivellato E, Nico B, Ribatti D (2008) The chromaffin vesicle: advances in understanding the composition of a versatile, multifunctional secretory organelle. Anat Rec (Hoboken) 291:1587–1602. CrossRef Medline

Del Castillo J, Katz B (1954) Quantal components of the end-plate potential. J Physiol 124:560–573. CrossRef Medline

de Wit H, Walter AM, Milosevic I, Gulyás-Kovács A, Riedel D, Sørensen JB, Verhage M (2009a) Synaptotagmin-1 docks secretory vesicles to syntaxin-1/SNAP-25 acceptor complexes. Cell 138:935–946. CrossRef Medline

de Wit J, Toonen RF, Verhage M (2009b) Matrix-dependent local retention of secretory vesicle cargo in cortical neurons. J Neurosci 29:23–37. CrossRef Medline

Duncan RR, Greaves J, Wiegand UK, Matskevich I, Bodammer G, Apps DK, Shipston MJ, Chow RH (2003) Functional and spatial segregation of secretory vesicle pools according to vesicle age. Nature 422:176–180. CrossRef Medline

Elhamdani A, Palfrey HC, Artalejo CR (2001) Quantal size is dependent on stimulation frequency and calcium entry in calf chromaffin cells. Neuron 31:819–830. CrossRef Medline

Fan F, Ji C, Wu Y, Ferguson SM, Tamarina N, Philipson LH, Lou X (2015) Dynamin 2 regulates biphasic insulin secretion and plasma glucose homeostasis. J Clin Invest 125:4026–4041. CrossRef Medline

Ferguson SM, De Camilli P (2012) Dynamin, a membrane-remodelling GTPase. Nat Rev Mol Cell Biol 13:75–88. CrossRef Medline

Ferguson SM, Brasnjo G, Hayashi M, Wölfel M, Collesi C, Giovedi S, Raimondi A, Gong LW, Ariel P, Paradise S, O'toole E, Flavell R, Cremona O, Miesenböck G, Ryan TA, De Camilli P (2007) A selective activity-dependent requirement for dynamin 1 in synaptic vesicle endocytosis. Science 316:570–574. CrossRef Medline

Fulop T, Radabaugh S, Smith C (2005) Activity-dependent differential

transmitter release in mouse adrenal chromaffin cells. J Neurosci 25: 7324–7332. CrossRef Medline

Gerachshenko T, Schwartz E, Bleckert A, Photowala H, Seymour A, Alford S (2009) Presynaptic G-protein-coupled receptors dynamically modify vesicle fusion, synaptic cleft glutamate concentrations, and motor behavior. J Neurosci 29:10221–10233. CrossRef Medline

González-Jamett AM, Báez-Matus X, Hevia MA, Guerra MJ, Olivares MJ, Martínez AD, Neely A, Cárdenas AM (2010) The association of dynamin with synaptophysin regulates quantal size and duration of exocytotic events in chromaffin cells. J Neurosci 30:10683–10691. CrossRef Medline

González-Jamett AM, Momboisse F, Guerra MJ, Ory S, Baez-Matus X, Barraza N, Calco V, Houy S, Couve E, Neely A, Martínez AD, Gasman S, Cárdenas AM (2013) Dynamin-2 regulates fusion pore expansion and quantal release through a mechanism that involves actin dynamics in neuroendocrine chromaffin cells. PLoS One 8:e70638. CrossRef Medline

He L, Wu LG (2007) The debate on the kiss-and-run fusion at synapses. Trends Neurosci 30:447–455. CrossRef Medline

Huang HP, Wang SR, Yao W, Zhang C, Zhou Y, Chen XW, Zhang B, Xiong W, Wang LY, Zheng LH, Landry M, Hökfelt T, Xu ZQ, Zhou Z (2007) Long latency of evoked quantal transmitter release from somata of locus coeruleus neurons in rat pontine slices. Proc Natl Acad Sci U S A 104: 1401–1406. CrossRef Medline

Jackson J, Papadopulos A, Meunier FA, McCluskey A, Robinson PJ, Keating DJ (2015) Small molecules demonstrate the role of dynamin as a bidirectional regulator of the exocytosis fusion pore and vesicle release. Mol Psychiatry 20:810–819. CrossRef Medline

Kuo ST, Wu QH, Liu B, Xie ZL, Wu X, Shang SJ, Zhang XY, Kang XJ, Liu LN, Zhu FP, Wang YS, Hu MQ, Xu HD, Zhou L, Liu B, Chai ZY, Zhang QF, Liu W, Teng SS, Wang CH, et al. (2014) Importing, caring, breeding, genotyping, and phenotyping a genetic mouse in a chinese university. J Mol Neurosci 53:487–492. CrossRef Medline

Larsen KE, Schmitz Y, Troyer MD, Mosharov E, Dietrich P, Quazi AZ, Savalle M, Nemani V, Chaudhry FA, Edwards RH, Stefanis L, Sulzer D (2006) Alpha-synuclein overexpression in PC12 and chromaffin cells impairs catecholamine release by interfering with a late step in exocytosis. J Neurosci 26:11915–11922. CrossRef Medline

Lou X, Paradise S, Ferguson SM, De Camilli P (2008) Selective saturation of slow endocytosis at a giant glutamatergic central synapse lacking dynamin 1. Proc Natl Acad Sci U S A 105:17555–17560. CrossRef Medline

Matsuda N, Lu H, Fukata Y, Noritake J, Gao H, Mukherjee S, Nemoto T, Fukata M, Poo MM (2009) Differential activity-dependent secretion of brain-derived neurotrophic factor from axon and dendrite. J Neurosci 29:14185–14198. CrossRef Medline

Mellander LJ, Trouillon R, Svensson MI, Ewing AG (2012) Amperometric post spike feet reveal most exocytosis is via extended kiss-and-run fusion. Sci Rep 2:907. CrossRef Medline

Miesenböck G, De Angelis DA, Rothman JE (1998) Visualizing secretion and synaptic transmission with pH-sensitive green fluorescent proteins. Nature 394:192–195. CrossRef Medline

Neher E, Sakaba T (2008) Multiple roles of calcium ions in the regulation of neurotransmitter release. Neuron 59:861–872. CrossRef Medline

Perrais D, Kleppe IC, Taraska JW, Almers W (2004) Recapture after exocytosis causes differential retention of protein in granules of bovine chromaffin cells. J Physiol 560:413–428. CrossRef Medline

Pothos EN, Przedborski S, Davila V, Schmitz Y, Sulzer D (1998) D2-like dopamine autoreceptor activation reduces quantal size in PC12 cells. J Neurosci 18:5575–5585. CrossRef Medline

Raghupathi R, Jessup CF, Lumsden AL, Keating DJ (2016) Fusion pore size limits 5-HT release from single enterochromaffin cell vesicles. J Cell Physiol 231:1593–1600. CrossRef Medline

Raimondi A, Ferguson SM, Lou X, Armbruster M, Paradise S, Giovedi S, Messa M, Kono N, Takasaki J, Cappello V, O'Toole E, Ryan TA, De Camilli P (2011) Overlapping role of dynamin isoforms in synaptic vesicle endocytosis. Neuron 70:1100–1114. CrossRef Medline

Ren L, Mellander LJ, Keighron J, Cans AS, Kurczy ME, Svir I, Oleinick A, Amatore C, Ewing AG (2016) The evidence for open and closed exocytosis as the primary release mechanism. Q Rev Biophys 49:e12. CrossRef Medline

Samasilp P, Chan SA, Smith C (2012) Activity-dependent fusion pore expansion regulated by a calcineurin-dependent dynamin-syndapin pathway in mouse adrenal chromaffin cells. J Neurosci 32:10438–10447. CrossRef Medline

Stevens CF, Williams JH (2000) "Kiss and run" exocytosis at hippocampal synapses. Proc Natl Acad Sci U S A 97:12828–12833. CrossRef Medline

Tsuboi T, McMahon HT, Rutter GA (2004) Mechanisms of dense core vesicle recapture following "kiss and run" ("cavicapture") exocytosis in insulin-secreting cells. J Biol Chem 279:47115–47124. CrossRef Medline

Wang C, Wang Y, Hu M, Chai Z, Wu Q, Huang R, Han W, Zhang CX, Zhou Z (2016) Synaptotagmin-11 inhibits clathrin-mediated and bulk endocytosis. EMBO Rep 17:47–63. CrossRef Medline

Wang Y, Wu Q, Hu M, Liu B, Chai Z, Huang R, Wang Y, Xu H, Zhou L, Zheng L, Wang C, Zhou Z (2017) Ligand- and voltage-gated Ca(2+) channels differentially regulate the mode of vesicular neuropeptide release in mammalian sensory neurons. Sci Signal 10:eaa1683. CrossRef Medline

Westerink RH, Ewing AG (2008) The PC12 cell as model for neurosecretion. Acta Physiol (Oxf) 192:273–285. CrossRef Medline

Wightman RM, Jankowski JA, Kennedy RT, Kawagoe KT, Schroeder TJ, Leszczyszyn DJ, Near JA, Diliberto EJ Jr, Viveros OH (1991) Temporally resolved catecholamine spikes correspond to single vesicle release from individual chromaffin cells. Proc Natl Acad Sci U S A 88:10754–10758. CrossRef Medline

Xia X, Lessmann V, Martin TF (2009) Imaging of evoked dense-core-vesicle exocytosis in hippocampal neurons reveals long latencies and kiss-and-run fusion events. J Cell Sci 122:75–82. CrossRef Medline

Zhang Q, Li Y, Tsien RW (2009) The dynamic control of kiss-and-run and vesicular reuse probed with single nanoparticles. Science 323:1448–1453. CrossRef Medline

Zhao WD, Hamid E, Shin W, Wen PJ, Krystofiak ES, Villarreal SA, Chiang HC, Kachar B, Wu LG (2016) Hemi-fused structure mediates and controls fusion and fission in live cells. Nature 534:548–552. CrossRef Medline

Zhou Z, Misler S (1995a) Amperometric detection of stimulus-induced quantal release of catecholamines from cultured superior cervical ganglion neurons. Proc Natl Acad Sci U S A 92:6938–6942. CrossRef Medline

Zhou Z, Misler S (1995b) Action potential-induced quantal secretion of catecholamines from rat adrenal chromaffin cells. J Biol Chem 270:3498–3505. CrossRef Medline

Zhou Z, Misler S, Chow RH (1996) Rapid fluctuations in transmitter release from single vesicles in bovine adrenal chromaffin cells. Biophys J 70: 1543–1552. CrossRef Medline

Zhu Y, Xu J, Heinemann SF (2009) Two pathways of synaptic vesicle retrieval revealed by single-vesicle imaging. Neuron 61:397–411. CrossRef Medline